



HAL
open science

Effect of saddle point anisotropy of point defects on their absorption by dislocations and cavities

Carpentier D., T. Jourdan, Y. Le Bouar, M.-C. Marinica

► **To cite this version:**

Carpentier D., T. Jourdan, Y. Le Bouar, M.-C. Marinica. Effect of saddle point anisotropy of point defects on their absorption by dislocations and cavities. *Acta Materialia*, 2017, 136, pp.323-334. 10.1016/j.actamat.2017.07.013 . hal-01632426

HAL Id: hal-01632426

<https://hal.science/hal-01632426>

Submitted on 5 Jul 2021

HAL is a multi-disciplinary open access archive for the deposit and dissemination of scientific research documents, whether they are published or not. The documents may come from teaching and research institutions in France or abroad, or from public or private research centers.

L'archive ouverte pluridisciplinaire **HAL**, est destinée au dépôt et à la diffusion de documents scientifiques de niveau recherche, publiés ou non, émanant des établissements d'enseignement et de recherche français ou étrangers, des laboratoires publics ou privés.



Distributed under a Creative Commons Attribution 4.0 International License

Effect of saddle point anisotropy of point defects on their absorption by dislocations and cavities

D. Carpentier^a, T. Jourdan^{a,*}, Y. Le Bouar^b, M.-C. Marinica^a

^a*DEN-Service de Recherches de Métallurgie Physique, CEA, Université Paris-Saclay, F-91191, Gif-sur-Yvette, France*

^b*LEM, CNRS/ONERA, 29 av. de la division Leclerc, 92322 Châtillon, France*

Abstract

Developing predictive models for the microstructure evolution of materials requires an accurate description of the point defects fluxes to the different sinks, such as dislocations, grain boundaries and cavities. This work aims at improving the evaluation of sink strengths of dislocations and cavities using object kinetic Monte-Carlo simulations parametrized with density functional theory calculations. The present accurate description of point defects migration enables quantitative assessment of the influence of the point defects anisotropy at saddle point. The results in aluminum show that the anisotropy at saddle point has a large influence on sink strengths. In particular, this anisotropy leads to the cavity being a biased sink. These results are explained by the analysis of the point defect trajectories to the sinks, which are shown to be strongly affected by the saddle point anisotropy.

Keywords: kinetic Monte Carlo, Diffusion, Irradiation, Dislocation, Cavity

1. Introduction

Supersaturation of point defects in metals occurs, for example, after plastic deformation [1], hydrogen charging [2, 3], solid or liquid state quenching [4, 5, 6] and irradiation [7]. This supersaturation leads to the formation of vacancy

*Corresponding author

Email address: thomas.jourdan@cea.fr (T. Jourdan)

5 clusters such as voids, stacking fault tetrahedra and dislocation loops and, in
6 the case of irradiation, self-interstitial clusters. These clusters are sinks for point
7 defects and grow, thereby affecting the macroscopic properties of materials.

8 Fluxes of point defects to the sinks of the microstructure strongly depend on
9 the elastic field created by the sinks, which modify the energy landscape. Strik-
10 ing examples of the role of elastic interactions between sinks and point defects
11 on the final microstructure come from materials under irradiation. Swelling [7]
12 and irradiation creep [8, 9] are due to a slight imbalance of absorption of point
13 defects (self-interstitial atoms (SIAs) and vacancies) by the different sinks of
14 the microstructure. In the so-called “dislocation bias model”, swelling is due to
15 the preferential absorption of interstitials by dislocations, which is responsible
16 for a net flux of vacancies to cavities [10]. In this model, cavities are assumed
17 to be neutral sinks, which means that they have no absorption bias for intersti-
18 tials. Some models for irradiation creep, such as SIPA (Stress Induced Preferred
19 Absorption), rely on the difference in climb velocity of different dislocation pop-
20 ulations, depending on their orientation with respect to the applied stress. In
21 such models, the climb velocity depends not only on the applied stress, but also
22 on the stress field created by the dislocations [8]. In order to simulate irradiation
23 induced phenomena such as swelling and creep, a proper description of the
24 effect of the elastic field created by sinks on point defect migration is therefore
25 crucial.

26 The simulation of long term microstructures under irradiation is conveniently
27 performed by rate equation cluster dynamics [11, 12, 13, 14]. In this kind of
28 mean-field model, the variation of the migration energy along the point defect
29 trajectory cannot be taken into account explicitly. The effect of elastic interac-
30 tions on point defect diffusion is found in the sink strengths for SIAs (k_i^2) and
31 vacancies (k_v^2). The bias, which is defined as the relative difference between the
32 sink strengths k_i^2 and k_v^2 , quantifies to what extent a sink preferentially absorbs
33 SIAs or vacancies, depending on its sign.

34 A large amount of data exists about sink strengths and bias values, but
35 the scattering is rather high. Assuming that dislocations are the only biased

36 sinks, the dislocation bias can be inferred from experimental swelling data,
37 using standard rate theory models [15, 16, 17, 18, 19]. However, swelling is
38 a combination of the bias and the fraction of freely migrating defects, which is
39 not precisely known for ion and neutron irradiations. Therefore, there is some
40 uncertainty about the bias values obtained by such methods. Depending on the
41 experimental data and the assumptions of the rate theory model, the dislocation
42 bias values typically range between 0.01 and 0.35. Sink strengths and biases can
43 also be computed. A common way is to solve the drift-diffusion equation for the
44 concentration of point defects around a sink. This method was used for the first
45 calculations, mostly for simple geometries and simple description of the sink-
46 point defect interaction [20, 21, 22, 23]. For more complex cases, phase field [24]
47 and object kinetic Monte Carlo (OKMC) simulations have been used [25, 26, 27].
48 OKMC methods are particularly handy to take into account the effect of elastic
49 interactions at stable and saddle points [28, 29].

50 The influence of elastic interactions at saddle position on the value of sink
51 strength was emphasized by Dederichs and Schroeder [30]. Although this ef-
52 fect had been discussed previously [31, 32, 33], these authors also suggested
53 that the *anisotropy* of point defects at saddle position could have an effect
54 on the sink strength. Such an effect was later confirmed for straight disloca-
55 tions [34, 35, 36, 37], infinitesimal dislocation loops [38] and voids [39]. However,
56 all these works contain approximations to make calculations tractable, so the
57 values of sink strengths significantly vary from one study to the other [37]. In
58 addition, the elastic dipoles of point defects are based on empirical potential cal-
59 culations, which are not always in agreement with first-principles calculations.
60 Only recently, the effect of saddle point anisotropy has been shown for the sink
61 strength of semi-coherent interfaces, using OKMC simulations parameterized
62 with density functional theory (DFT) calculations [29].

63 In the present work, we perform OKMC simulations to study the sink
64 strengths of straight dislocations and spherical cavities in pure aluminum, in
65 order to assess the role of saddle point anisotropy. To that purpose, the elas-
66 tic interactions between sinks and point defects are modeled explicitly in the

67 OKMC code. Point defects are represented by their elastic dipole tensors com-
 68 puted by DFT calculations.

69 This paper is structured as follows. Section 2 describes the method used to
 70 calculate sink strengths. Section 3 presents the study of the straight dislocation.
 71 The case of a spherical cavity is treated in section 4.

72 2. Methods

73 2.1. OKMC simulations and sink strength calculation

74 Sink strengths are calculated with an OKMC code [29], allowing the simula-
 75 tion of many point defect trajectories in an efficient way, and making it possible
 76 to account for the point defects properties and elastic interactions between point
 77 defects and sinks [28, 40, 29]. A single type of sink is introduced in the simula-
 78 tion box. It can be a dislocation or a spherical cavity. The sinks are considered
 79 as immobile and remain unchanged after absorption of defects. The temper-
 80 ature is set to 300 K. At this temperature, thermal equilibrium concentration
 81 of point defects is far smaller than the concentration imposed by irradiation.
 82 Therefore, thermal generation of point defects by the sinks is neglected.

83 SIAs and vacancies are considered separately, in dedicated simulations, thus
 84 no recombination is possible. They are generated uniformly at a constant cre-
 85 ation rate G_0 (in s^{-1}), and migrate inside the box by performing atomic jumps
 86 until they are absorbed by the sink. The migrating point defects do not react
 87 with each other to form clusters and no long-range interactions between point
 88 defects are considered. Periodic boundary conditions are used in all 3 dimen-
 89 sions. Point defects are considered as absorbed by the sink when the distance
 90 d between the sink center and the point defect verifies $d \leq d_{\text{reac}}$ where d_{reac} is
 91 the reaction distance depending on the nature of the sink.

92 To increment the simulation time, a residence time algorithm is used [41, 42].
 93 At a given time t , the time step is given by $\Delta t = -\ln(r_1)/\Gamma_{\text{tot}}$ where r_1 is a
 94 random number chosen in $]0, 1]$ and Γ_{tot} is the sum of the frequencies of all N_e
 95 possible events, *i. e.* $\Gamma_{\text{tot}} = \sum_{i=0}^{N_e-1} \Gamma_i$. The possible events are the creation

96 of a point defect due to irradiation (frequency $\Gamma_0 = G_0$) or an atomic jump
 97 from a stable position to a neighboring one (frequency Γ_i , $i = 1, \dots, N_e -$
 98 1). The chosen event j is such that $\sum_{i=0}^{j-1} \Gamma_i < r_2 \Gamma_{\text{tot}} \leq \sum_{i=0}^j \Gamma_i$, with r_2
 99 a random number chosen in $]0, 1]$. Frequencies of atomic jumps are given by
 100 $\Gamma_i = \nu_0 \exp(-\Delta E_i / (k_B T))$, with ν_0 the attempt frequency assumed to be the
 101 same for all jumps, k_B is the Boltzmann constant, T the temperature and $\Delta E_i =$
 102 $E_i^{\text{sad}} - E_i^{\text{sta}}$ the difference of energy between the saddle point of the jump and
 103 the initial stable position.

The energy of point defects at stable point E_i^{sta} and at saddle point E_i^{sad}
 are given by

$$E_i^{\text{sta}} = - \sum_{j,k} P_{i,jk}^{\text{sta}} \epsilon_{jk}(\mathbf{r}_i^{\text{sta}}) \quad (1)$$

$$E_i^{\text{sad}} = E^{\text{m}} - \sum_{j,k} P_{i,jk}^{\text{sad}} \epsilon_{jk}(\mathbf{r}_i^{\text{sad}}), \quad (2)$$

104 where E^{m} is the migration energy without elastic interactions and \mathbf{P}^{sta} and
 105 \mathbf{P}^{sad} are elastic dipole tensors (\mathbf{P} -tensors) describing the point defects at stable
 106 and saddle positions, respectively [43, 44]. The saddle position \mathbf{r}^{sad} is simply
 107 considered as the midpoint along the reaction coordinate between the two stable
 108 positions involved in the jump. The strain, written ϵ , is generated by the
 109 sink. Since we focus on the effect of saddle point anisotropy, we consider that
 110 \mathbf{P} -tensors do not depend on the local strain, *i. e.* we neglect polarisability
 111 effects [43]. Other energy terms, such that higher order terms in the multipole
 112 expansion [44] and image interactions for voids [45, 46], are also neglected.

113 In our simulations, unless otherwise specified, the calculations are performed
 114 in isotropic elasticity, using available analytical expressions of the strain pro-
 115 duced by the sink. This assumption is expected to be reasonable in the case of
 116 face centered cubic (FCC) aluminum, studied here, because the elastic moduli
 117 tensor of this material is only weakly anisotropic (see Tab. 1). This makes it
 118 possible to focus on the effect of point defects anisotropy only. However, to check
 119 the influence of the anisotropy of the elastic moduli tensor on the sink strength,
 120 simulations are also performed in anisotropic elasticity, using the values of elas-

121 tic constants given in [47]. In that case, a Fast Fourier Transform (FFT)-based
 122 method is used to compute the strain field at mechanical equilibrium [48, 49, 50].

Elastic moduli tensor terms and Zener anisotropy ratio [47]			
C_{11} (GPa)	C_{12} (GPa)	C_{44} (GPa)	$A = 2C_{44}/(C_{11} - C_{12})$
106.51	60.38	27.8	1.21
Constants for isotropic elasticity			
Poisson's ratio ν		Shear modulus μ (GPa)	
0.35		25.91	

Table 1: Elastic constants of aluminum at 300 K. The isotropic elastic constants are calculated from the tensor terms by the Voigt average [51].

In the mean field rate theory, the sink strength k^2 defines the ability of a sink to absorb point defects. In this formalism, the evolution equation of the average number of defects \bar{N} is given by

$$\frac{d\bar{N}}{dt} = G_0 - k^2 D \bar{N}, \quad (3)$$

with D the point defect diffusion coefficient, which reads

$$D = \alpha a_0^2 \nu_0 \exp\left(-\frac{E^m}{k_B T}\right). \quad (4)$$

123 In this equation, $\alpha = \frac{2}{3}$ for SIAs ($\langle 100 \rangle$ dumbbells) and $\alpha = 1$ for vacancies,
 124 and a_0 is the lattice parameter of the FCC lattice.

The absorption of point defects by the sink is expressed in Eq. (3) through the second term in the right-hand side. When the steady state is reached, the sink strength can be computed by

$$k^2 = \frac{G_0}{D \bar{N}}. \quad (5)$$

Two sink strength values are obtained, k_{SIA}^2 for SIAs and k_{vac}^2 for vacancies. From these two values, the sink bias B can be calculated by [52]

$$B = \frac{k_{\text{SIA}}^2 - k_{\text{vac}}^2}{k_{\text{SIA}}^2}. \quad (6)$$

125 This parameter describes the ability of the sink to absorb more SIAs than va-
 126 cancies.

127 In the OKMC simulations, the number of point defects in the box N is
 128 recorded every 10^4 steps. At the end of the simulation, the average number of
 129 defects at steady state \bar{N} is computed by averaging the recorded values. The sink
 130 strengths and bias values are then computed using Eqs. (5)–(6). The simulated
 131 times are chosen to obtain sufficient accuracy on the value of \bar{N} , and thus on k^2 .
 132 A block-averaging procedure [53] is used to compute the error estimates σ on
 133 the sink strength and bias. In the following, the error bars in figures correspond
 134 to $\pm 3\sigma$.

135 2.2. Representation of point defects

136 To compute interactions between the sink and the point defects, the \mathbf{P} -
 137 tensors at stable points \mathbf{P}^{sta} and at saddle points \mathbf{P}^{sad} are needed. The values
 138 of \mathbf{P} -tensors for SIAs and vacancies in aluminum are computed by DFT cal-
 139 culations. The DFT simulation cell for SIA/vacancy contains 256 ± 1 atoms.
 140 Calculations are performed with VASP code using the projector augmented wave
 141 framework [54, 55, 56, 57]. The plane wave energy cutoff is set to 450 eV and the
 142 Hermite-Gaussian broadening-width for Brillouin zone integration is 0.2 eV. The
 143 calculations are performed including the s semi-core states $[\text{Ne}]3s^23p^1$. The ex-
 144 change correlation energy is evaluated using the Perdew-Burke-Ernzerhof (PBE)
 145 Generalized Gradient Approximation (GGA) [58]. The k -point grid mesh is set
 146 to shifted $3 \times 3 \times 3$ grid. Each configuration is relaxed using the gradient con-
 147 jugate technique. The climbing image method [59] using 15 images is used in
 148 order to localize the saddle point. In relaxed configurations, minimum or saddle
 149 point, the forces on each atom are lower than $0.001 \text{ eV}/\text{\AA}$. With such settings
 150 the relative error in the energy and \mathbf{P} -tensor components is estimated to be less
 151 than 0.5% and 4%, respectively, from converged values [29].

152 For the configurations illustrated in Tab. 2, the following results are obtained:

153 1. For SIAs, migration energy of $E^{\text{m}} = 0.105 \text{ eV}$, and

- 154 • at stable point, dumbbell along $[100]$:

$$\mathbf{P}_{\text{SIA,ref}}^{\text{sta}} = \begin{bmatrix} 19.652 & 0 & 0 \\ 0 & 18.518 & 0 \\ 0 & 0 & 18.518 \end{bmatrix} \text{ eV} \quad (7)$$

- 155 • at saddle point, for a [100]-to-[010] migration path:

$$\mathbf{P}_{\text{SIA,ref}}^{\text{sad}} = \begin{bmatrix} 19.498 & 1.133 & 0 \\ 1.133 & 19.498 & 0 \\ 0 & 0 & 19.034 \end{bmatrix} \text{ eV} \quad (8)$$

- 156 2. For vacancies, migration energy of $E^{\text{m}} = 0.605$ eV and

- 157 • at stable point:

$$\mathbf{P}_{\text{vac,ref}}^{\text{sta}} = \begin{bmatrix} -3.238 & 0 & 0 \\ 0 & -3.238 & 0 \\ 0 & 0 & -3.238 \end{bmatrix} \text{ eV} \quad (9)$$

- 158 • at saddle point, for a migration along the [110] direction:

$$\mathbf{P}_{\text{vac,ref}}^{\text{sad}} = \begin{bmatrix} -2.866 & -0.080 & 0 \\ -0.080 & -2.866 & 0 \\ 0 & 0 & 1.000 \end{bmatrix} \text{ eV} \quad (10)$$

159 These values show that SIAs are weakly anisotropic at stable and saddle
 160 points, while vacancies are perfectly isotropic at stable point and strongly
 161 anisotropic at saddle point. The anisotropy of SIAs at stable point is in ex-
 162 cellent agreement with the experimental value $|P_{11} - P_{22}| = 1.1 \pm 0.3$ eV [60].
 163 The relaxation volumes at stable point for interstitials and vacancies, deduced
 164 from the trace of the dipole tensor through $\Delta V^{\text{sta}} = \text{Tr}(\mathbf{P})/3K$ with K the
 165 bulk modulus, seem slightly overestimated: they are equal to -0.40Ω for va-
 166 cancies and 2.35Ω for interstitials (Ω is the atomic volume), while experimental
 167 values range from -0.05 to -0.38Ω for vacancies and are equal to $1.9 \pm 0.4 \Omega$
 168 for interstitials [61, 62].

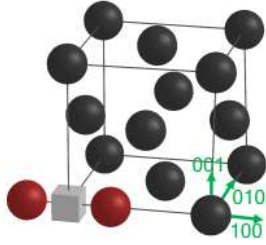
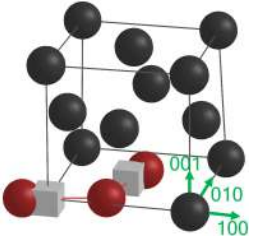
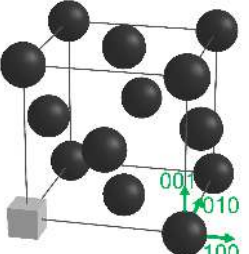
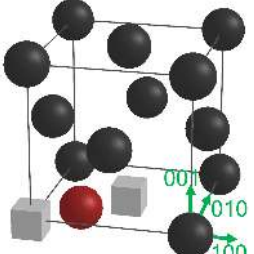
	Stable position	Saddle position
SIA		
vac		

Table 2: Schematic representations of stable and saddle positions of point defects in FCC lattice, with orientations corresponding to the \mathbf{P} -tensors in Eqs. (7) to (10). Here, black spheres represent the regular lattice atomic positions, red spheres represent atomic positions outside of lattice nodes and gray cubes represent vacancies.

169 To understand which properties of point defects have a major influence on
 170 the sink strengths, different simulation cases are built, using the previous \mathbf{P} -
 171 tensors or simplified versions of them. The cases are given in Tab. 3.

172 The first case (case 0, $\mathbf{P}_0^{\text{sta}} = \mathbf{0}$ and $\mathbf{P}_0^{\text{sad}} = \mathbf{0}$) is considered as a reference
 173 to validate the method used in this work, by comparing the calculated sink
 174 strengths to the corresponding analytical solutions. Indeed, for the boundary
 175 conditions considered here, the analytical expressions only exist when the sink
 176 strain field is not considered, *i. e.* when the point defects do not interact with
 177 the sink.

178 An accurate assessment of the effects of elastic interactions on the sink
 179 strength is done using the real point defect description (case 2, $\mathbf{P}_2^{\text{sta}} = \mathbf{P}_{\text{ref}}^{\text{sta}}$
 180 and $\mathbf{P}_2^{\text{sad}} = \mathbf{P}_{\text{ref}}^{\text{sad}}$).

The following two approximations 2' and 2'' are used to identify the point defect properties influencing the sink strengths. Case 2' corresponds to point defects with isotropic dipole tensors at saddle point but with the same relaxation volume as for case 2:

$$\mathbf{P}_{2'}^{\text{sta}} = \mathbf{P}_{\text{ref}}^{\text{sta}} \quad (11)$$

$$\mathbf{P}_{2'}^{\text{sad}} = \frac{1}{3} \text{Tr}(\mathbf{P}_{\text{ref}}^{\text{sad}}) \mathbf{I}, \quad (12)$$

where \mathbf{I} is the identity tensor. Such an approximation permits to enlighten the effect of saddle point anisotropy by comparing results to case 2. For case 2'', a further approximation is used: dipole tensors are taken isotropic at stable point, with the same relaxation volume as cases 2 and 2':

$$\mathbf{P}_{2''}^{\text{sta}} = \frac{1}{3} \text{Tr}(\mathbf{P}_{\text{ref}}^{\text{sta}}) \mathbf{I} \quad (13)$$

$$\mathbf{P}_{2''}^{\text{sad}} = \frac{1}{3} \text{Tr}(\mathbf{P}_{\text{ref}}^{\text{sad}}) \mathbf{I}. \quad (14)$$

181 Therefore, by comparing cases 2' and 2'', the effect of anisotropy at stable point
182 can be evaluated.

Finally, a traditional approximation in the calculation of sink strengths consists in ignoring the differences in point defect properties at stable and saddle points. Defect properties are given solely by the relaxation volume at stable point ΔV^{sta} [52, 63, 22, 64, 23]. This is tantamount to using the following dipole tensors (case 1):

$$\mathbf{P}_1^{\text{sta}} = \mathbf{P}_1^{\text{sad}} = \frac{1}{3} \text{Tr}(\mathbf{P}_{\text{ref}}^{\text{sta}}) \mathbf{I}. \quad (15)$$

183 3. Straight dislocation

184 3.1. Case definition

185 The simulation box contains two dislocations, each dislocation having the
186 following characteristics: line vector $\mathbf{l} = \frac{1}{\sqrt{6}} [\bar{1} \bar{1} \bar{2}]$, vector normal to the glide
187 plane $\mathbf{n} = \frac{1}{\sqrt{3}} [1 \ 1 \ \bar{1}]$ and Burgers vector $\mathbf{b} = \pm \frac{a_0}{2} [\bar{1} \ 1 \ 0]$ ($\|\mathbf{b}\| = \frac{a_0}{\sqrt{2}}$). This

		SIA	vacancy
Case 0	Non interacting defects	$\mathbf{P}_{\text{SIA}}^{\text{sta}} = \mathbf{0}$ $\mathbf{P}_{\text{SIA}}^{\text{sad}} = \mathbf{0}$	$\mathbf{P}_{\text{vac}}^{\text{sta}} = \mathbf{0}$ $\mathbf{P}_{\text{vac}}^{\text{sad}} = \mathbf{0}$
Case 1	Spherical inclusions	$\mathbf{P}_{\text{SIA}}^{\text{sta}} = 18.896 \mathbf{I}$ $\mathbf{P}_{\text{SIA}}^{\text{sad}} = 18.896 \mathbf{I}$	$\mathbf{P}_{\text{vac}}^{\text{sta}} = -3.238 \mathbf{I}$ $\mathbf{P}_{\text{vac}}^{\text{sad}} = -3.238 \mathbf{I}$
Case 2	Real defects	$\mathbf{P}_{\text{SIA}}^{\text{sta}} = \begin{bmatrix} 19.652 & 0 & 0 \\ 0 & 18.518 & 0 \\ 0 & 0 & 18.518 \end{bmatrix}$ $\mathbf{P}_{\text{SIA}}^{\text{sad}} = \begin{bmatrix} 19.498 & 1.133 & 0 \\ 1.133 & 19.498 & 0 \\ 0 & 0 & 19.034 \end{bmatrix}$	$\mathbf{P}_{\text{vac}}^{\text{sta}} = -3.238 \mathbf{I}$ $\mathbf{P}_{\text{vac}}^{\text{sad}} = \begin{bmatrix} -2.866 & -0.080 & 0 \\ -0.080 & -2.866 & 0 \\ 0 & 0 & 1.000 \end{bmatrix}$
Case 2'	Defects simplified at saddle points	$\mathbf{P}_{\text{SIA}}^{\text{sta}} = \begin{bmatrix} 19.652 & 0 & 0 \\ 0 & 18.518 & 0 \\ 0 & 0 & 18.518 \end{bmatrix}$ $\mathbf{P}_{\text{SIA}}^{\text{sad}} = 19.343 \mathbf{I}$	$\mathbf{P}_{\text{vac}}^{\text{sta}} = -3.238 \mathbf{I}$ $\mathbf{P}_{\text{vac}}^{\text{sad}} = -1.577 \mathbf{I}$
Case 2''	Defects simplified at stable and saddle points	$\mathbf{P}_{\text{SIA}}^{\text{sad}} = 18.896 \mathbf{I}$ $\mathbf{P}_{\text{SIA}}^{\text{sad}} = 19.343 \mathbf{I}$	$\mathbf{P}_{\text{vac}}^{\text{sad}} = -3.238 \mathbf{I}$ $\mathbf{P}_{\text{vac}}^{\text{sad}} = -1.577 \mathbf{I}$

Table 3: \mathbf{P} -tensors for the different simulation cases. The values are given in eV, for the configuration illustrated in Tab. 2. For vacancies, as they are isotropic at stable point, cases 2' and 2'' are identical.

188 corresponds to a perfect straight edge dislocation in the aluminum FCC lattice.
189 The capture radius of the straight dislocations is set to $r_c = 2\|\mathbf{b}\|$, which means
190 that for each dislocation $d_{\text{reac}} = 2\|\mathbf{b}\|$ [65, 20].

191 The two edge dislocations of opposite Burgers vectors are introduced in an
192 orthorhombic simulation box, according to the configuration in Fig. 1. There-
193 fore, the dislocation density only depends on the box dimensions according to
194 $\rho = \frac{2}{d_x \cdot d_y}$, so different densities can be studied by varying the box dimensions
195 (keeping the aspect ratio constant). The lattice is rotated to ensure that the
196 dislocation line vector is aligned with the z -direction of the box, while the Burg-
197 ers vectors are aligned with the x -direction. Such a configuration ensures that
198 the strain is continuous at the simulation box borders. Other configurations
199 could have been studied, a few have been tested and the configuration choice
200 does not alter the method nor the generality of our results.

201 As illustrated in Fig. 2, due to the periodic boundary conditions, the con-

202 figuration is equivalent to a 2D array of dislocations in the xy -plane. To cal-
 203 culate the strain field, we have to sum along x the strain fields of infinite y -
 204 columns of dislocations with alternate Burgers vectors, noted ϵ^+ and ϵ^- for
 205 $\mathbf{e}_x \cdot \mathbf{b} > 0$ and $\mathbf{e}_x \cdot \mathbf{b} < 0$, respectively. The strain field generated by an in-
 206 finite row of dislocations ϵ^\pm is given in [66] and [51]. The complete strain
 207 field is then given by summing the contributions of neighboring boxes $\epsilon(x, y) =$
 208 $\sum_{k=-N}^N (\epsilon^+(x + k \cdot d_x, y) + \epsilon^-(x + k \cdot d_x, y))$, using a sufficiently large value for
 209 N to reach convergence. We have used $N = 1$, which gives a relative error on
 210 the strain lower than 10^{-3} .

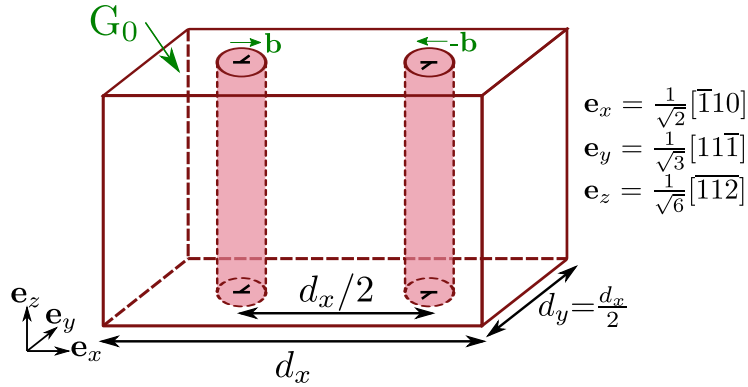


Figure 1: Configuration of the simulation box containing two edge dislocations, with opposite Burgers vectors.

211 3.2. Sink strength and bias

212 Values of the sink efficiency $Z = k^2/\rho$ and of the bias for dislocation den-
 213 sities from $5 \cdot 10^{13} \text{ m}^{-2}$ to 10^{16} m^{-2} , encompassing the densities in irradiated
 214 materials [67], are shown in Fig. 3.

215 The reliability of our approach is proved by the good agreement between the
 216 results obtained in the case of non interacting defects (case 0, yellow squares)
 217 and the analytical expression [68]. We have verified that the small differences
 218 are due to the different boundary conditions at the capture radius r_c . Indeed,
 219 the analytical treatment assumes that the concentration of point defects is zero
 220 at exactly $r = r_c$, while for the OKMC simulations, the defects are only removed

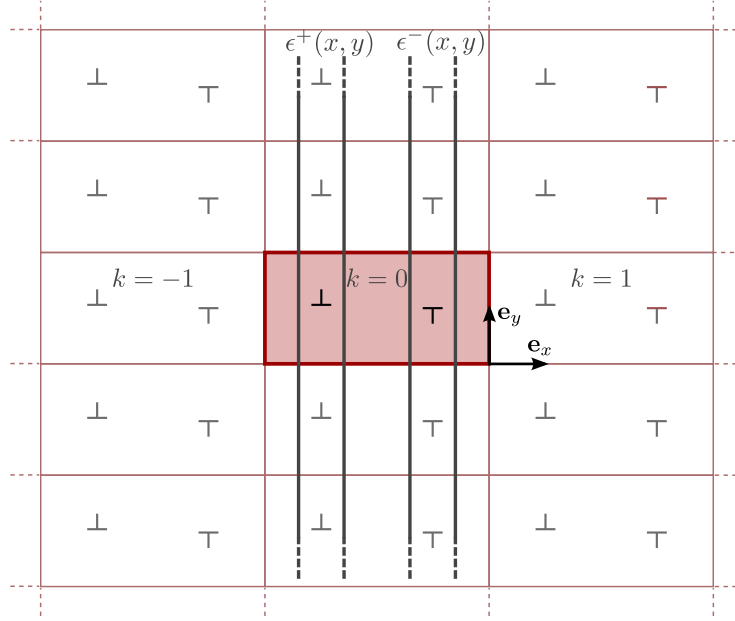


Figure 2: Schematic representation of the calculation of the strain with periodic boundary conditions. The strains ϵ^+ and ϵ^- are generated by the columns associated to the edge dislocations with the Burgers vectors \mathbf{b} such that $\mathbf{e}_x \cdot \mathbf{b} > 0$ and $\mathbf{e}_x \cdot \mathbf{b} < 0$, respectively.

221 after the last atomic jump that enters the capture region $r \leq r_c$, so the concen-
 222 tration is zero for some value lower than r_c . As proposed in [69, 25, 70], this
 223 difference can be accounted for by using an effective capture radius \tilde{r}_c slightly
 224 smaller than r_c in the analytical formula to mimic the OKMC configuration.

225 When the complete \mathbf{P} -tensors are used (case 2 – real defects, gray down-
 226 pointing triangles), sink strengths for vacancies are twice higher than the values
 227 obtained when the elastic interactions are neglected, for the highest dislocation
 228 densities studied. This increase is even more important for SIAs than for vacan-
 229 cies, and the difference increases with the dislocation density. This leads to a
 230 strongly positive bias value, increasing with the dislocation density.

231 To identify the properties of point defects responsible for the sink strength
 232 variation, the dipole tensors are modified. By removing the anisotropy of the
 233 elastic dipole tensors at the saddle point (case 2'), the sink strength is reduced for
 234 both types of point defects. The decrease is particularly important for vacancies,

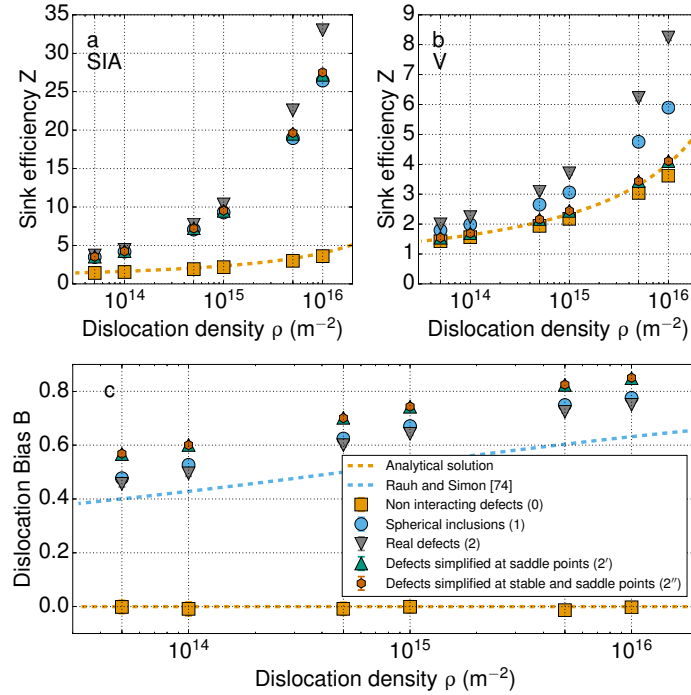


Figure 3: Straight dislocation sink efficiency for (a) SIAs and (b) vacancies, (c) bias. The error bars are displayed for all values, some of them are too small to be visible.

235 which are very anisotropic at saddle point. This shows that the saddle point
 236 anisotropy is responsible for a significant variation of the sink strength, through
 237 the decrease of the migration barriers near the dislocation.

238 The influence of stable point anisotropy can be assessed by comparing the
 239 latter results for case 2' to the results for case 2'' (defects simplified at stable
 240 and saddle points). Removing the anisotropy at stable points does not modify
 241 the sink strength values, and consequently leaves the bias unchanged. This
 242 shows that the anisotropy at stable point has no influence on the sink strength
 243 and sink bias in aluminum. This is due to the fact that, in this material, the
 244 anisotropy at stable point for SIAs is quite small, while vacancies are isotropic.

245 In Fig. 3 we also show the sink strength obtained when point defects have
 246 the same properties at stable and saddle points based on the relaxation volume

247 at stable point (case 1, blue disks). The sink strengths are indeed quite different
 248 from the ones obtained for case 2. For SIAs, the sink strength is close to the
 249 one obtained for cases 2' and 2'', due to the fact that the relaxation volumes
 250 at saddle points are similar: for case 1, $\frac{1}{3} \text{Tr}(\mathbf{P}_{\text{SIA}}^{\text{sad}}) = 18.896$ eV and for cases
 251 2' and 2'', $\frac{1}{3} \text{Tr}(\mathbf{P}_{\text{SIA}}^{\text{sad}}) = 19.343$ eV. On the contrary, the relaxation volumes
 252 at saddle points for vacancies vary a lot between case 1 and cases 2' and 2'':
 253 for case 1, $\frac{1}{3} \text{Tr}(\mathbf{P}_{\text{vac}}^{\text{sad}}) = -3.238$ eV and for cases 2' and 2'', $\frac{1}{3} \text{Tr}(\mathbf{P}_{\text{vac}}^{\text{sad}}) =$
 254 -1.577 eV. Consequently, the interactions are stronger for the vacancies in case
 255 1 than in cases 2' and 2'', giving a stronger sink strength. The dislocation bias
 256 obtained in case 1 is close to the one obtained for real dipole tensors (case 2),
 257 but this is completely incidental. Finally, various analytical expressions exist
 258 in the literature for case 1, but for isolated dislocations and different boundary
 259 conditions [71, 72, 73, 74]. In Fig. 3 we plot the solution provided by Rauh and
 260 Simon [74], which corresponds to the case of prescribed concentration on the
 261 system boundary (other expressions of the sink strengths correspond to slightly
 262 different boundary conditions, see Ref. [23] for a discussion of this point and a
 263 comparison of the formulas). It is shown that the results agree qualitatively but
 264 the analytical bias values are smaller than the OKMC values. Reasons for this
 265 discrepancy are given in Appendix A.

266 These results reveal the strong effect of elastic interactions, and more partic-
 267 ularly show that the saddle point anisotropy of point defects is a key parameter
 268 for the variation of the sink strength and bias.

269 3.3. Analysis and discussion

270 In the previous section we stated that the decreasing migration barriers near
 271 the dislocation, due to the saddle point anisotropy, leads to a significant increase
 272 in the sink strengths, especially for the vacancy. These numerical results are
 273 compared with previous analytical calculations, using various approximations.
 274 These previous studies were done in copper. However, due to similar point
 275 defect properties in aluminum and copper, trends are expected to be alike in
 276 both materials. The first estimation of the effect of saddle point anisotropy

277 was obtained by Skinner and Woo [36]. To make the calculations tractable,
278 they transformed the diffusion problem into a cylindrically symmetric one and
279 assumed that the diffusion coefficient only depends on one component of the
280 dipole tensor. They concluded that the effect was small and led to a slight
281 increase in the sink strengths for vacancies and interstitials. With an arbitrary
282 choice of the point defect anisotropy and diffusion tensor, Chen showed that the
283 effect of anisotropy could be described by an effective relaxation volume [35].
284 The increase of the relaxation volume due to the anisotropy at saddle point is
285 such that the effect on the sink strength is rather large. Borodin and Ryazanov
286 did not resort to some of the assumptions made by Skinner and Woo [37] and
287 obtained a few percents decrease of the sink strength for interstitials and an
288 increase of about 20 % for vacancies. More recently, Sivak and Sivak [75] showed
289 with OKMC calculations that the anisotropy of vacancies at saddle point is
290 responsible for complex variations of the sink strength with the dislocation type.
291 Here, by exactly taking into account the interaction between the dislocation and
292 the point defect at saddle position, we show that an increase of about 20 % for
293 interstitials and 100 % for vacancies can be obtained with respect to an isotropic
294 defect.

295 We have also shown that the anisotropy of interstitials at stable point does
296 not change the bias value. Several authors have pointed out that if the concen-
297 tration at the boundary of the simulation cell is imposed, fluxes, and therefore
298 sink strengths, do not depend on the stable point energy [30, 36, 37]. Therefore,
299 in this case, no effect of defect anisotropy at stable point is expected. Here, the
300 situation is different, since we impose the creation rate of defects and measure
301 the sink strength by the average concentration in the simulation cell (Eq. (5)).
302 The concentration depends on the stable point energy, so the sink strength can
303 potentially depend on the point defect anisotropy at stable position [76]. How-
304 ever, the anisotropy of interstitials is so low that the difference in energy between
305 the isotropic and the anisotropic cases is negligible, leading to no appreciable
306 effect on the sink strength.

307 To have a better understanding of the influence of the saddle point anisotropy,

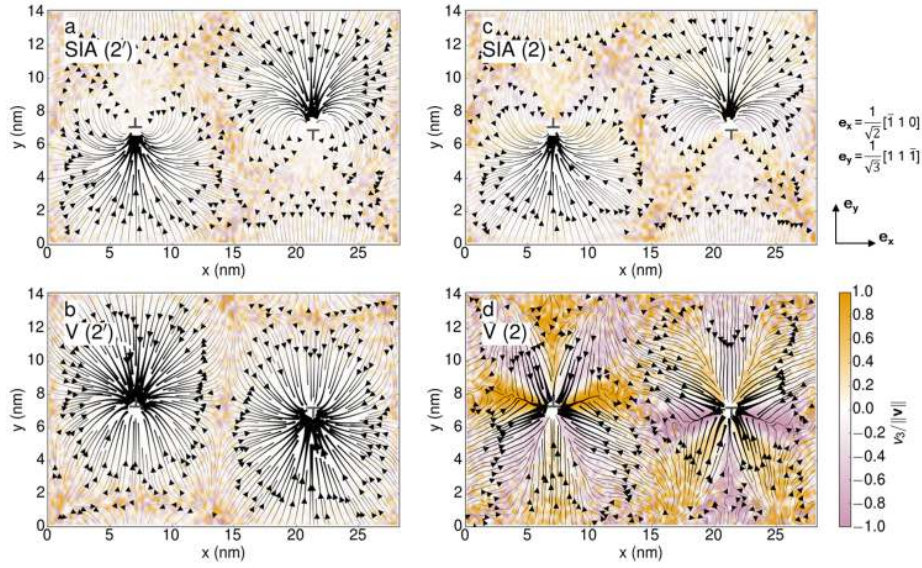


Figure 4: Average fluxes of (a) SIAs and (b) vacancies with isotropic saddle points (case 2'), and (c) SIAs and (d) vacancies with real \mathbf{P} -tensors (case 2). The flux $\mathbf{v} = (v_1, v_2, v_3)$ is recorded through surfaces between stable positions. The color corresponds to the component of the flux in the z -direction ($v_3/\|\mathbf{v}\|$), and the lines represent the flux in the xy plane $\mathbf{v}_{xy} = (v_1, v_2)$. The width of the lines is here proportional to the norm of the flux $\|\mathbf{v}\| = \sqrt{v_1^2 + v_2^2 + v_3^2}$.

308 the migration paths of point defects to the dislocations can be extracted from
 309 OKMC simulations. The fluxes of point defects are recorded through dividing
 310 surfaces between stable atomic positions during OKMC simulations. From these
 311 data, average migration paths are obtained. The result is represented in Fig. 4.

312 Results for point defects with isotropic saddle points (case 2') are shown
 313 in Fig. 4 a-b. As expected, SIAs migrate and reach the dislocations through
 314 their dilated sides and are repelled from the compressed sides. On the contrary,
 315 vacancies mostly flow to the compressed sides. The difference is less clear than
 316 for interstitials, due to the lower magnitude of the elastic interactions.

317 When the saddle point anisotropy is taken into account (case 2), we obtain
 318 the fluxes in Fig. 4 c-d. These graphs show that the saddle point anisotropy
 319 not only has an influence on the sink strength but also on the point defects

320 trajectories. Vacancies now migrate to the dislocations to enter through the
 321 lateral sides along the Burgers vector direction ($\pm \mathbf{e}_x$). The difference is not so
 322 visible for SIAs, as the relative importance of the deviatoric component of their
 323 dipole tensors is smaller than for vacancies.

In the case of vacancies, the saddle point anisotropy also gives rise to non-zero component of the flux along the dislocation line direction. Note, however, that by symmetry the flux averaged in the xy -plane is zero in this direction. The fluxes along the dislocation line direction can be explained using the diffusion tensor, whose terms can be written [30]

$$D_{ij}(\mathbf{r}) = \frac{1}{2} \nu_0 \sum_{\mathbf{h}} h_i h_j \exp\left(-\frac{E_{\mathbf{h}}^{\text{sad}}(\mathbf{r}) - E^{\text{sta}}(\mathbf{r})}{k_{\text{B}}T}\right), \quad (16)$$

where (see Eqs. (1)–(2))

$$E^{\text{sta}}(\mathbf{r}) = -\sum_{k,l} P_{kl}^{\text{sta}} \epsilon_{kl}(\mathbf{r}) \quad (17)$$

$$E_{\mathbf{h}}^{\text{sad}}(\mathbf{r}) = E^{\text{m}} - \sum_{k,l} P_{\mathbf{h},kl}^{\text{sad}} \epsilon_{kl}(\mathbf{r} + \mathbf{h}/2). \quad (18)$$

324 In these equations, \mathbf{h} refers to the possible jumps from a stable position \mathbf{r}
 325 to the neighboring one $\mathbf{r} + \mathbf{h}$. These possible jumps are represented in Fig. 5.

In the case of an isotropic saddle point (case 2'), $P_{\mathbf{h},kl}^{\text{sad}} = P_{kl}^{\text{sad}}$. In addition, if we assume that $\epsilon_{kl}(\mathbf{r} + \mathbf{h}/2) \approx \epsilon_{kl}(\mathbf{r})$, the saddle point energy $E_{\mathbf{h}}^{\text{sad}}(\mathbf{r})$ no longer depends on the jump and the diffusion tensor becomes

$$D_{ij}(\mathbf{r}) = \frac{1}{2} \nu_0 \exp\left(-\frac{E^{\text{sad}}(\mathbf{r}) - E^{\text{sta}}(\mathbf{r})}{k_{\text{B}}T}\right) \sum_{\mathbf{h}} h_i h_j. \quad (19)$$

Since

$$\sum_{\mathbf{h}} h_i h_j = 0 \quad \text{if } i \neq j, \quad (20)$$

326 an isotropic saddle point leads to a diagonal diffusion tensor. This conclusion
 327 also holds for a non uniform strain field, if it is expanded to first order in \mathbf{h} .

On the contrary, this simplification cannot be made when the saddle point

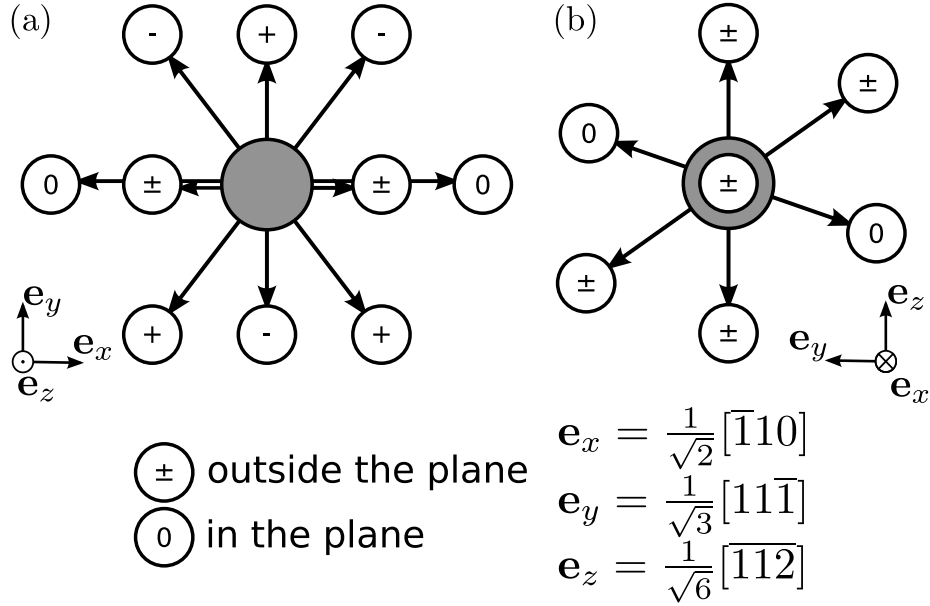


Figure 5: Lattice stable position (gray sphere) and its first nearest neighbor positions (white spheres). Representation (a) in the xy plane and (b) in the yz plane of the simulation box.

dipole tensor is anisotropic. The diffusion tensor terms D_{ij} then depend on

$$\sum_{\mathbf{h}} h_i h_j \exp\left(-\frac{P_{\mathbf{h},kl}^{\text{sad}} \epsilon_{kl}(\mathbf{r} + \mathbf{h}/2)}{k_B T}\right) \approx \sum_{\mathbf{h}} h_i h_j \exp\left(-\frac{P_{\mathbf{h},kl}^{\text{sad}} \epsilon_{kl}(\mathbf{r})}{k_B T}\right). \quad (21)$$

328 Because the strain has a different coupling with each jump \mathbf{h} , the lattice symme-
 329 try is lowered and the different jumps in Fig. 5 no longer cancel each other out.
 330 Non-zero off-diagonal terms, in particular D_{xz} and D_{yz} , can therefore appear
 331 and lead to flux components along the dislocation line direction.

The presence of such a flux component may have some implications on the effect of external stress on dislocation sink strengths. It has been found that the point defect anisotropy at saddle point induces a stress dependence of the dislocation sink strength, known as the “stress-induced preferential absorption due to anisotropic diffusion” (SIPA-AD) [34, 36, 37]. This phenomenon has been shown to be more than one order of magnitude larger than the usual SIPA effect,

noted SIPA-I, due to the polarisability of point defects [36, 77]. Assessing the relative importance of both mechanisms is crucial in order to describe properly irradiation creep for example. For a uniaxial stress, SIPA-AD manifests itself through a dependency of the sink strength on the direction of the stress with respect to the dislocation line. For the sake of simplicity, let us consider the migration of the vacancy in an xy -plane perpendicular to the dislocation line. The saddle point energy reads

$$E^{\text{sad}}(\boldsymbol{\epsilon}^{\text{a}}) = E^{\text{sad}}(0) - P_1^{\text{sad}}\epsilon_{x'x'}^{\text{a}} - P_2^{\text{sad}}\epsilon_{y'y'}^{\text{a}} - P_3^{\text{sad}}\epsilon_{zz}^{\text{a}}, \quad (22)$$

where $\boldsymbol{\epsilon}^{\text{a}}$ is the applied strain, expressed here in the basis $(\mathbf{e}_{x'}, \mathbf{e}_{y'}, \mathbf{e}_z)$ where \mathbf{P}^{sad} is diagonal, and $P_1^{\text{sad}} = -2.946$ eV, $P_2^{\text{sad}} = -2.786$ eV and $P_3^{\text{sad}} = 1.000$ eV are the three eigenvalues of \mathbf{P}^{sad} (see Eq. (10)). If a tensile stress is applied along the dislocation line (\mathbf{e}_z), the energy becomes

$$E^{\text{sad}}(\boldsymbol{\epsilon}^{\text{a}}) = E^{\text{sad}}(0) - 2.946\nu\epsilon^{\text{a}} - 2.786\nu\epsilon^{\text{a}} - 1.000\epsilon^{\text{a}}. \quad (23)$$

If the stress is in the plane, for example along $\mathbf{e}_{x'}$, it reads

$$E^{\text{sad}}(\boldsymbol{\epsilon}^{\text{a}}) = E^{\text{sad}}(0) + 2.946\nu\epsilon^{\text{a}} - 2.786\nu\epsilon^{\text{a}} + 1.000\epsilon^{\text{a}}. \quad (24)$$

332 Therefore it is easily seen that providing vacancies migrate in a plane normal
 333 to the dislocation line, a tensile stress along the line will decrease the migration
 334 barrier and thus increase the sink strength, whereas a tensile stress in the jump
 335 direction will have the opposite effect. If the vacancy does not migrate in this
 336 plane, the effect can be lower. In the works dealing with SIPA-AD, the large
 337 magnitude of the SIPA-AD effect has been obtained by assuming that point
 338 defect fluxes are perpendicular to the dislocation line [36, 77]. However, we
 339 have seen that when a three-dimensional model is used, saddle point anisotropy
 340 leads to fluxes with components along the dislocation line. Therefore, it is not
 341 clear whether the magnitude of the SIPA-AD will remain as large compared to
 342 SIPA-I. Additional work is needed to evaluate precisely the importance of both
 343 mechanisms, by studying specifically different stress levels and directions [78].

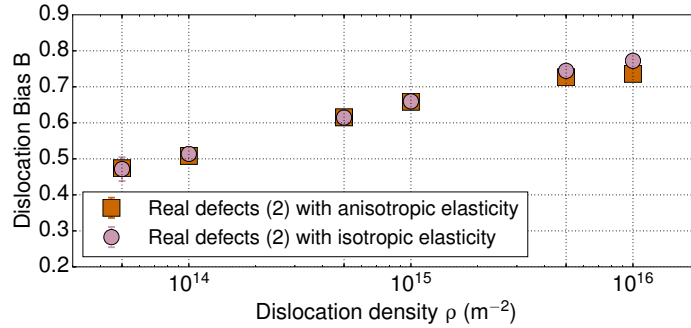


Figure 6: Dislocation bias obtained for real defects (case 2) with interpolation of the analytical solution in Fourier space for the strain, with isotropic and anisotropic elasticity.

344 3.4. Importance of elastic moduli tensor anisotropy

345 Point defect anisotropy at saddle point has been identified as one of the main
 346 parameters influencing the sink strength value in isotropic elasticity. Although
 347 aluminum is a weakly anisotropic material ($A = 1.21$, see Tab. 1), it can be
 348 worth investigating the effect of the anisotropy of the elastic moduli tensor on
 349 the sink strength.

350 The results obtained for the dislocation bias are presented in Fig. 6. In this
 351 figure, both results are obtained with calculations using the analytical solution
 352 in Fourier space for the strain field [48, 49, 50]. With anisotropic elasticity, only
 353 a small variation of the bias values can be observed. It is much less important
 354 than the variation induced by the saddle point anisotropy. The influence of the
 355 elastic moduli tensor anisotropy is therefore far less important than the one of
 356 the point defect anisotropy. Consequently, as far as aluminum is concerned,
 357 the calculations can be done with isotropic elasticity. A similar conclusion was
 358 drawn in the case of iron, for which it was seen that the change in the sink
 359 strength is lower than 10% when elastic constants are changed from their values
 360 at 0 K ($A = 2.3$) to the ones at 1000 K ($A = 4.5$) [79].

361 **4. Spherical cavity**

362 *4.1. Case definition*

363 To compute the cavity sink strengths and bias, the cubic simulation box
 364 of size d contains a single centered spherical cavity, as illustrated in Fig. 7.
 365 This cavity is a perfect sink with a constant radius r_c , with a capture radius of
 366 $d_{\text{reac}} = r_c + r_{\text{PD}}$ where r_{PD} is the point defect radius ($r_{\text{PD}} = 0.16$ nm). The
 367 cavity density only depends on the box dimensions and is given by $\rho = 1/d^3$, so
 368 different densities can be studied by varying the box dimension d .

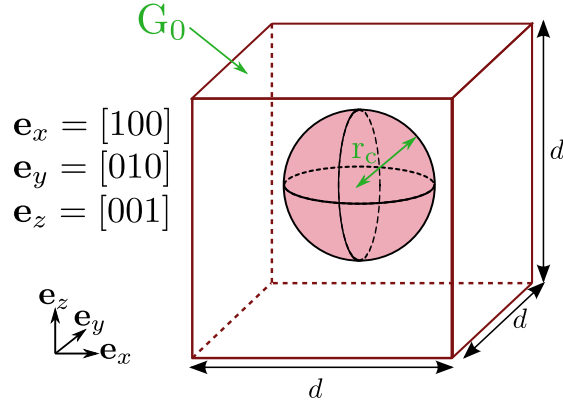


Figure 7: Configuration of the simulation box containing a spherical cavity.

The strain field generated by a cavity is calculated after the expressions given in [80, 39]:

$$\epsilon_{ij}(\mathbf{r}) = \frac{\left(-\frac{2\gamma}{r_c}\right)}{4\mu} \left(\frac{r_c}{r}\right)^3 \left(\delta_{ij} - \frac{3x_i x_j}{r^2}\right). \quad (25)$$

369 In this equation, μ is the shear modulus of the material, the coordinates in
 370 the box x, y, z are noted x_1, x_2, x_3 for convenience, with $r = \sqrt{x_1^2 + x_2^2 + x_3^2}$,
 371 and γ is the surface tension, set to the typical value of $1 \text{ J}\cdot\text{m}^{-2}$ [39].

372 From Eq. (25), it can be seen that $\text{Tr}(\epsilon) = 0$. As a consequence, for defects
 373 having an isotropic dipole tensor $\mathbf{P} = P_0 \mathbf{I}$, the energy induced by the elastic
 374 field is $E = -P_0 \text{Tr}(\epsilon) = 0$. Therefore when both vacancies and SIAs have
 375 isotropic dipole tensors, e.g. in the usual approximation of case 1, the bias is
 376 zero, and the cavity is a neutral sink.

377 The simulations involving defects with isotropic dipole tensors at both stable
 378 and saddle points (case 1 and case 2') are then equivalent to case 0, with
 379 no interactions. Consequently, only the cases of non interacting defects (case
 380 0), real defects (case 2) and defects simplified at saddle points (case 2') are
 381 considered here.

382 *4.2. Sink strength and bias*

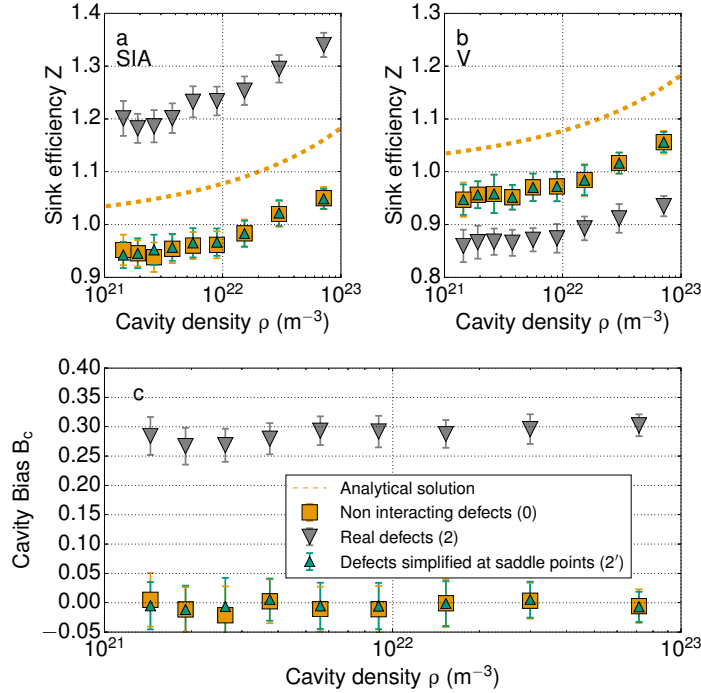


Figure 8: Cavity sink efficiency for (a) SIAs and (b) vacancies, (c) bias, for a cavity of radius 1 nm.

The cavity sink strength and bias are calculated for a cavity of radius $r_c = 1$ nm, for a density between 10^{21} and 10^{23} cavities per m^3 , corresponding to densities commonly measured in irradiated materials [67]. The sink efficiencies Z are then calculated by

$$Z = \frac{k^2}{4\pi d_{\text{reac}} \rho}. \quad (26)$$

383 Results are presented in Fig. 8.

384 As in the case of dislocations, a good agreement is obtained between the sink
 385 strengths for non interacting defects (case 0, yellow squares) and the analytical
 386 expression for the cavity sink strength [68], validating our approach. The small
 387 difference can be explained by the boundary conditions at the cavity surface, in
 388 the same way as for the dislocation.

389 It is particularly interesting to notice how the elastic interactions influence
 390 the sink strength values. The results obtained for real defects (case 2, gray down-
 391 pointing triangles) show that the interactions increase the cavity sink strength
 392 for SIAs, but slightly reduce the sink strength for vacancies as compared to the
 393 case without elastic interactions. This yields a positive bias of 0.3 in average for
 394 the densities studied. The bias weakly depends on the cavity density, because of
 395 the short range of interactions. This bias value shows that the cavity cannot be
 396 considered as a neutral sink when the elastic interactions are taken into account.

397 The sink strengths obtained for point defects with isotropic saddle points
 398 (case 2', green triangles) are equal to the ones obtained for non interacting de-
 399 fects, so the bias is zero. Therefore, results show that the saddle point anisotropy
 400 of point defects alone is responsible for the increase of the bias value. The sta-
 401 ble point anisotropy does not influence the sink strength nor the bias, which is
 402 consistent with the results obtained for the dislocation.

403 Fig. 9 presents the cavity bias for a density of $3.74 \cdot 10^{21} \text{ m}^{-3}$, for cavity radii
 404 from 1 nm to 5 nm, with consideration of point defects anisotropy (case 2). The
 405 cavity bias decreases when the cavity radius increases due to the decrease in
 406 $1/r_c$ in Eq. (25), but even for a radius of 5 nm the bias is still above 0.1, which
 407 indicates that the cavity is a biased sink.

408 *4.3. Analysis and discussion*

409 In the same way as for dislocations, cavity sink strengths have been deter-
 410 mined by analytical calculations, taking into account the diffusion anisotropy [39].
 411 With different boundary conditions as those used in our simulations, and under
 412 the assumptions that the cavity is small with respect to the simulation cell and

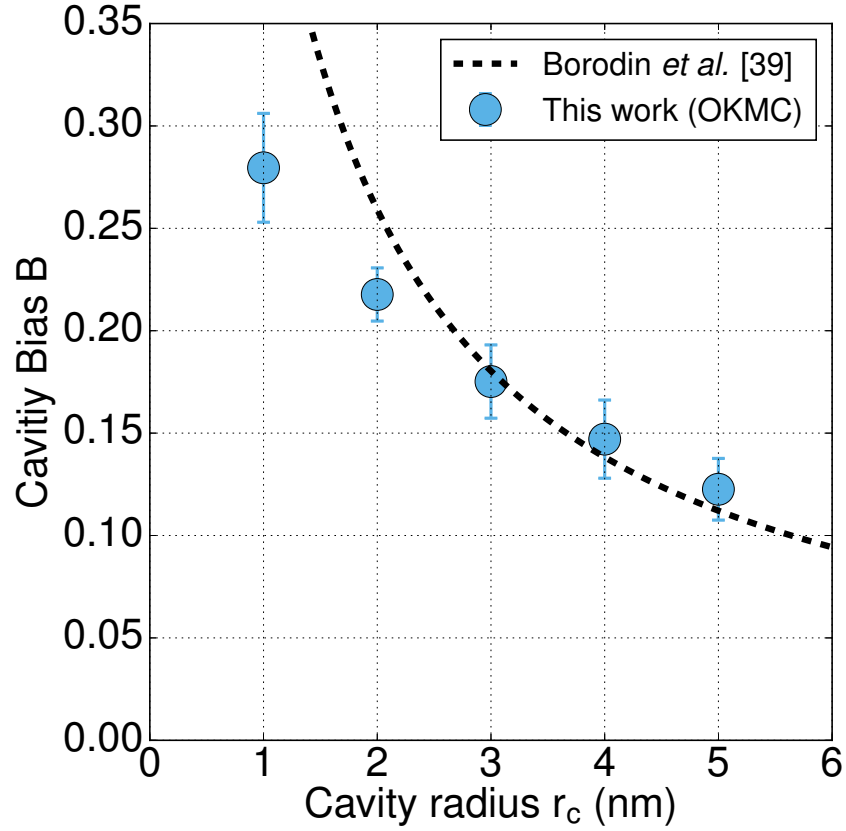


Figure 9: Cavity bias B as a function of the cavity radius r_c , for real defects (case 2), and the analytical expression computed from [39]. The cavity density is $3.74 \cdot 10^{21} \text{ m}^{-3}$.

413 that the strain is low, the expression obtained for the sink strength is remark-
 414 ably simple: it depends on the components of the dipole tensor and varies as
 415 $1/r_c$. The bias values obtained from these expressions are represented in Fig. 9.
 416 This analytical expression is in agreement with our simulation results for the
 417 larger cavities, but the values differ for the small radii, for which the strain field
 418 is stronger. For our simulation parameters, these calculations show that for a
 419 cavity of radius 1 nm, the sink strength for vacancies is reduced by a factor 0.69
 420 when the anisotropy at saddle point is taken into account, while the one for

421 SIAs increases by a factor 1.29. In our simulations, the reduction for vacancies
 422 is less marked, whereas the value for SIAs is very close. Therefore, the bias
 423 value is higher in the analytical approach ($B = 0.46$).

424 More in-depth investigation of the effect of saddle point anisotropy can be
 425 obtained by extracting point defect trajectories. They are represented in Fig. 10
 426 in the xy -plane, for both isotropic (case 2', a-b) and anisotropic (case 2, c-
 427 d) saddle points. In the case of isotropic saddle point, the average fluxes of
 428 both SIAs and vacancies are normal to the cavity. This corresponds to the
 429 fluxes that would be obtained without interactions between point defects and
 430 the sink. When the saddle point is anisotropic, trajectories of SIAs are not
 431 markedly changed. On the contrary, trajectories of vacancies are curved close
 432 to the cavity.

433 Fig. 11 presents the probability of absorption on the surface of the cavity
 434 for a radius of 1 nm. These results confirm that the probability of absorption of
 435 SIAs is almost homogeneous on the cavity surface, with a small increase along
 436 the $\langle 111 \rangle$ directions. On the contrary, Fig. 11-b shows that the probability of
 437 absorption of vacancies is strongly anisotropic. Vacancies are absorbed almost
 438 only through the $\langle 100 \rangle$ directions. In a similar way, anisotropic concentration
 439 fields around the cavity were found by Borodin *et al.* [39]. Qualitatively, it can
 440 be explained by the curvature of the point defect trajectories (Fig. 10-d), which
 441 converge to the $\langle 100 \rangle$ directions. In general, as emphasized in the case of the
 442 dislocation, vacancies tend to migrate more easily if the strain along the jump
 443 direction is negative (such defects are called “F-type defects” by Woo [38]).
 444 Tangential strain due to the cavity is negative, while normal strain is positive.
 445 Therefore, defects tend to migrate tangentially close to the cavity, which reduces
 446 the point defect absorption and the sink strength. This effect is more or less
 447 strong, depending on the orientation of jumps with respect to the strain field
 448 of the cavity. This lattice effect is a signature of the saddle point anisotropy.
 449 In order to more precisely assess this trajectory curvature effect very near to
 450 the cavity, more involved simulations, including other energy terms that may
 451 be important at low distance [45], should be performed.

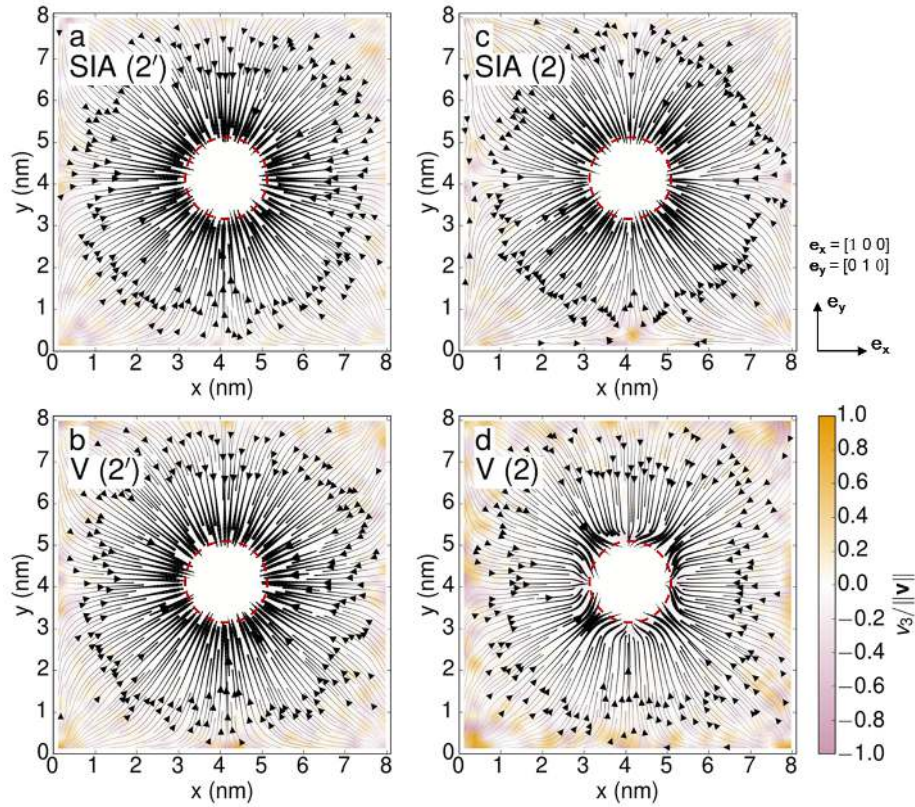


Figure 10: Average fluxes of (a) SIAs and (b) vacancies with isotropic saddle points (case 2'), and (c) SIAs and (d) vacancies with real \mathbf{P} -tensors (case 2). The same convention is applied as in Fig. 4.

452 5. Conclusion

453 In this work, OKMC simulations have been performed to evaluate sink
 454 strengths and bias values of a straight dislocation and of a spherical cavity
 455 in aluminum. The elastic interactions between the sink and the migrating point
 456 defects are explicitly modeled and the point defects are represented by their
 457 elastic dipole tensors (\mathbf{P} -tensors), which are computed by DFT calculations.
 458 The influence of the saddle point anisotropy on the sink strengths and bias has
 459 been quantitatively assessed.

460 Results show that the values of sink strengths and bias are strongly increased

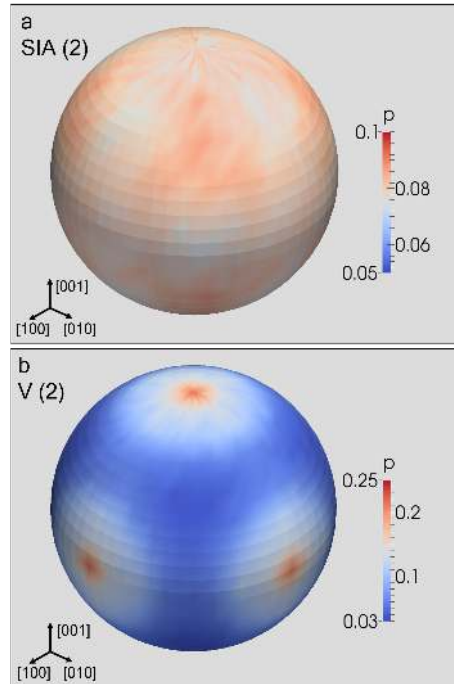


Figure 11: Probability density of absorption p of (a) SIAs and (b) vacancies (case 2) on the surface of the cavity, for a cavity radius of 1 nm.

461 by the elastic interactions, for both the dislocation and the cavity. The study
 462 of the different approximations of the \mathbf{P} -tensors highlights the influence of the
 463 saddle point anisotropy of defects. It leads to the cavity being a biased sink with
 464 a bias of almost 0.3 for a radius of 1 nm, which reduces as the radius increases.

465 The influence of the saddle point anisotropy has been enlightened by the
 466 study of the point defects migration paths. We have shown that the saddle
 467 point anisotropy leads to more complex trajectories than in the isotropic case,
 468 especially for vacancies which have a more anisotropic saddle point than in-
 469 terstitials. Near the dislocation, vacancies migrate along the Burgers vector
 470 direction, and not only through the compressed side. The vacancy flux has a
 471 non-zero component along the dislocation line direction. Near a cavity, vacan-
 472 cies tend to migrate tangentially and be absorbed through the $\langle 100 \rangle$ directions,
 473 while the absorption of SIAs is nearly isotropic.

474 Similar results are expected for other FCC metals, as dipole tensors have
 475 the same features [29]. These results have implications on swelling and irradiation
 476 creep rates, and also suggest that the saddle point anisotropy of vacancies
 477 could play a significant role in many FCC based materials, in particular when
 478 solidification, heat treatments and/or deformation processes have led to a super-
 479 saturation of vacancies. In addition, this anisotropy could be of importance
 480 in coherent multi-phase materials, such as nickel based superalloys, in which va-
 481 cancies diffuse in an inhomogeneous strain field resulting from both the internal
 482 multiphase microstructure and the thermo-mechanical treatment.

483 **Appendix A. Comparison of OKMC results and analytical calcula-** 484 **tions for straight dislocations (case 1)**

485 In this section we compare the OKMC results for case 1 (spherical inclu-
 486 sions), for straight dislocations, with the analytical calculation provided by Rauh
 487 and Simon [74]. This analytical study corresponds to a single dislocation with
 488 a prescribed concentration at a distance R from the dislocation position. The
 489 effect of the strain field of other dislocations is therefore not taken into account.

490 In order to explain the discrepancy observed in Fig. 3, the drift-diffusion
 491 equation has also been solved on two different cases (Fig. A.12), using the fi-
 492 nite element (FE) method. More details about the methodology can be found
 493 in Ref. [23]. In the first case (Fig. A.12-(a)), the concentration is imposed at
 494 the outer boundary of the computation domain, corresponding to the analyt-
 495 ical treatment from [74]. The sink strength is deduced from the flux to the
 496 dislocation. In the second case (Fig. A.12-(b)), a source term is imposed, cor-
 497 responding to our OKMC simulations. The sink strength is deduced from the
 498 average concentration of defects, using Eq. (5). In both cases, the effect of the
 499 strain field of surrounding dislocations is taken into account.

500 Results are compared in Fig. A.13. A very good agreement is obtained
 501 between FE simulations with imposed creation rate and OKMC simulations.
 502 On the contrary, FE simulations with imposed concentration tends to the an-

503 analytical solution for low dislocation densities, whereas they depart from each
 504 other as the dislocation density increases. This means that the discrepancy
 505 between the analytical solution and the OKMC results mostly comes from the
 506 different boundary conditions, whereas at high dislocation densities the effect
 507 of surrounding dislocation strain fields also plays a role in the difference.

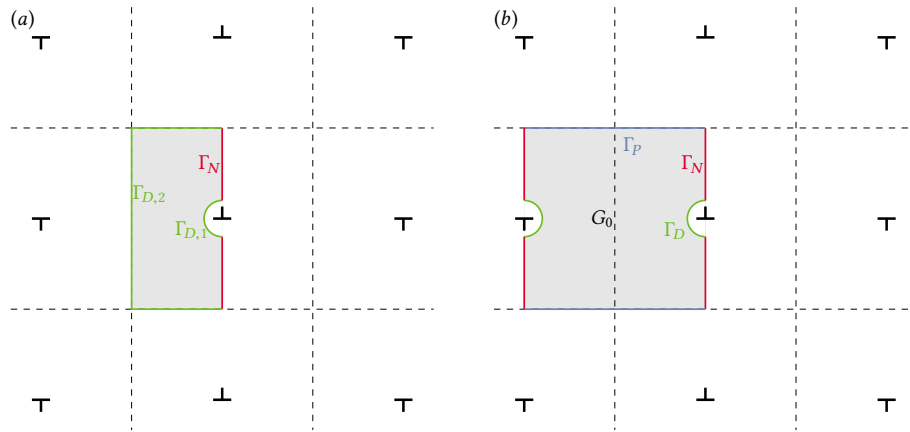


Figure A.12: Computation domains for FE calculations (in grey). (a) Concentration is imposed on the outer boundary ($\Gamma_{D,2}$). Concentration is zero on $\Gamma_{D,1}$ and the normal flux is zero on Γ_N . (b) Creation rate G_0 is imposed in the volume. Concentration is zero on Γ_D , the normal flux is zero on Γ_N and periodic boundary conditions are used on Γ_P .

- 508 [1] S. H. Goods, L. M. Brown, The nucleation of cavities by plastic deformation,
 509 Acta Metall. 27 (1979) 1.
- 510 [2] V. G. Gavriljuk, V. N. Bugaev, Y. N. Petrov, A. V. Tarasenko, Hydrogen-
 511 induced equilibrium vacancies in fcc iron-base alloys, Scr. Mater. 34 (1996)
 512 903.
- 513 [3] T. Neeraj, R. Srinivasan, J. Li, Hydrogen embrittlement of ferritic steels:
 514 Observations on deformation microstructure, nanoscale dimples and failure
 515 by nanovoiding, Acta Mater. 60 (2012) 5160.
- 516 [4] J. Takamura, Quenched-in vacancies and quenching strains in gold, Acta
 517 Metall. 9 (1961) 547.

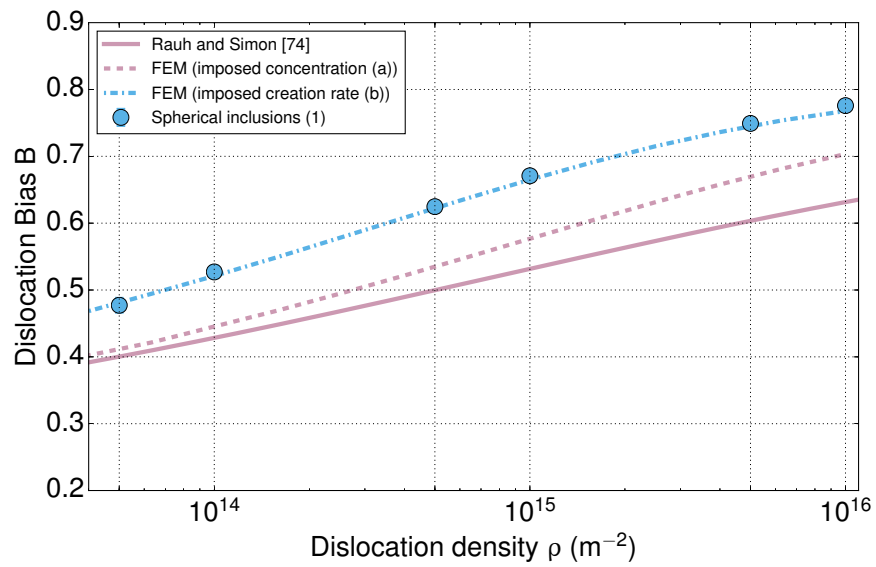


Figure A.13: Bias of straight dislocations when point defects are considered as spherical inclusions (case 1), obtained with various approaches: analytical calculation by Rauh and Simon [74], FE calculations with two different boundary conditions and OKMC calculations.

- 518 [5] P. B. Hirsch, J. Silcox, R. E. Smallman, K. H. Westmacott, Dislocation
519 loops in quenched aluminum, *Philos. Mag.* 3 (1958) 897.
- 520 [6] G. Thomas, R. H. Willens, Defects in aluminum quenched from the liquid
521 state, *Acta Metall.* 12 (1964) 191.
- 522 [7] G. W. Greenwood, A. J. E. Foreman, D. E. Rimmer, The role of vacancies
523 and dislocations in the nucleation and growth of gas bubbles in irradiated
524 fissile materials, *J. Nucl. Mater.* 4 (1959) 305.
- 525 [8] P. T. Heald, M. V. Speight, Steady-state irradiation creep, *Philos. Mag.*
526 29 (1974) 1075.
- 527 [9] L. K. Mansur, Irradiation creep by climb-enabled glide of dislocations
528 resulting from preferred absorption of point defects, *Philos. Mag. A* 39
529 (1979) 497.
- 530 [10] A. D. Brailsford, R. Bullough, The rate theory of swelling due to void
531 growth in irradiated metals, *J. Nucl. Mater.* 44 (1972) 121.
- 532 [11] S. I. Golubov, A. M. Ovcharenko, A. V. Barashev, B. N. Singh, Grouping
533 method for the approximate solution of a kinetic equation describing the
534 evolution of point-defect clusters, *Philos. Mag. A* 81 (2001) 643.
- 535 [12] A. Hardouin-Duparc, C. Moingeon, N. Smetniansky-de-Grande, A. Barbu,
536 Microstructure modelling of ferritic alloys under high flux 1 MeV electron
537 irradiations, *J. Nucl. Mater.* 302 (2002) 143.
- 538 [13] D. Xu, B. D. Wirth, M. Li, M. A. Kirk, Combining in situ transmission
539 electron microscopy irradiation experiments with cluster dynamics model-
540 ing to study nanoscale defect agglomeration in structural materials, *Acta*
541 *Mater.* 60 (2012) 4286.
- 542 [14] T. Jourdan, G. Bencteux, G. Adjanor, Efficient simulation of kinetics of
543 radiation induced defects: A cluster dynamics approach, *J. Nucl. Mater.*
544 444 (2014) 298.

- 545 [15] M. J. Makin, G. P. Walters, A. J. E. Foreman, The void swelling behaviour
546 of electron irradiated type 316 austenitic steel, *J. Nucl. Mater.* 95 (1980)
547 155.
- 548 [16] G. P. Walters, The electron irradiation of pure Fe-Cr-Ni alloys in temper-
549 ature range 400 to 700°C, *J. Nucl. Mater.* 136 (1985) 263.
- 550 [17] S. I. Golubov, B. N. Singh, H. Trinkaus, On recoil-energy-dependent defect
551 accumulation in pure copper Part II. Theoretical treatment., *Philos. Mag.*
552 A 81 (2001) 2533.
- 553 [18] T. Okita, W. G. Wolfer, A critical test of the classical rate theory for void
554 swelling, *J. Nucl. Mater.* 327 (2004) 130.
- 555 [19] Z. Chang, P. Olsson, D. Terentyev, N. Sandberg, Dislocation bias factors in
556 fcc copper derived from atomistic calculations, *J. Nucl. Mater.* 441 (2013)
557 357.
- 558 [20] C. H. Woo, W. S. Liu, M. S. Wuschke, A Finite-difference Calculation of
559 Point Defect Migration into a Dislocation Loop, Technical Report AECL-
560 6441, Atomic Energy of Canada Limited, 1979.
- 561 [21] R. Bullough, D. W. Wells, J. R. Willis, M. H. Wood, The interaction energy
562 between interstitial atoms and dislocations and its relevance to irradiation
563 damage processes, in: M. F. Ashby, R. Bullough, C. S. Hartley, J. P. Hirth
564 (Eds.), *Dislocation Modelling of Physical Systems*, Pergamon, 1981, p. 116.
- 565 [22] V. I. Dubinko, A. S. Abyzov, A. A. Turkin, Numerical evaluation of the
566 dislocation loop bias, *J. Nucl. Mater.* 336 (2005) 11.
- 567 [23] T. Jourdan, Influence of dislocation and dislocation loop biases on mi-
568 crostructures simulated by rate equation cluster dynamics, *J. Nucl. Mater.*
569 467 (2015) 286.
- 570 [24] H. Rouchette, L. Thuinet, A. Legris, A. Ambard, C. Domain, Quantitative
571 phase field model for dislocation sink strength calculations, *Comp. Mater.*
572 *Sci.* 88 (2014) 50.

- 573 [25] H. L. Heinisch, B. N. Singh, S. I. Golubov, The effects of one-dimensional
574 glide on the reaction kinetics of interstitial clusters, *J. Nucl. Mater.* 283
575 (2000) 737.
- 576 [26] L. Malerba, C. S. Becquart, C. Domain, Object kinetic Monte Carlo study
577 of sink strengths, *J. Nucl. Mater.* 360 (2007) 159.
- 578 [27] V. Jansson, L. Malerba, A. De Backer, C. S. Becquart, C. Domain, Sink
579 strength calculations of dislocations and loops using OKMC, *J. Nucl.*
580 *Mater.* 442 (2013) 218.
- 581 [28] A. B. Sivak, V. M. Chernov, V. A. Romanov, P. A. Sivak, Kinetic Monte-
582 Carlo simulation of self-point defect diffusion in dislocation elastic fields in
583 bcc iron and vanadium, *J. Nucl. Mater.* 417 (2011) 1067.
- 584 [29] A. Vattré, T. Jourdan, H. Ding, M.-C. Marinica, M. J. Demkowicz, Non-
585 random walk diffusion enhances the sink strength of semicoherent inter-
586 faces, *Nat. Commun.* 7 (2016) 10424.
- 587 [30] P. H. Dederichs, K. Schroeder, Anisotropic diffusion in stress fields, *Phys.*
588 *Rev. B* 17 (1978) 2524.
- 589 [31] J. S. Koehler, Diffusion of lattice defects in a stress field, *Phys. Rev.* 181
590 (1969) 1015.
- 591 [32] H. K. Birnbaum, B. L. Eyre, W. Drotning, The effect of diffusivity gradients
592 on diffusion to dislocations, *Philos. Mag.* 23 (1971) 847.
- 593 [33] K. Schroeder, K. Dettmann, Diffusion reactions in long range potentials,
594 *Z. Phys. B* 22 (1975) 343.
- 595 [34] C. N. Tomé, H. A. Cecatto, E. J. Savino, Point-defect diffusion in a strained
596 crystal, *Phys. Rev. B* 25 (1982) 7428.
- 597 [35] I.-W. Chen, Anisotropic diffusion of point defects to edge dislocations, *J.*
598 *Nucl. Mater.* 125 (1984) 52.

- 599 [36] B. C. Skinner, C. H. Woo, Shape effect in the drift diffusion of point defects
600 into straight dislocations, *Phys. Rev. B* 30 (1984) 3084.
- 601 [37] V. A. Borodin, A. I. Ryazanov, The effect of diffusion anisotropy on dislo-
602 cation bias and irradiation creep in cubic lattice materials, *J. Nucl. Mater.*
603 210 (1994) 258.
- 604 [38] C. H. Woo, Intrinsic bias differential between vacancy loops and interstitial
605 loops, *J. Nucl. Mater.* 107 (1982) 20.
- 606 [39] V. A. Borodin, A. I. Ryazanov, C. Abromeit, Void bias factors due to the
607 anisotropy of the point defect diffusion, *J. Nucl. Mater.* 207 (1993) 242.
- 608 [40] G. Subramanian, D. Perez, B. P. Uberuaga, C. N. Tomé, A. F. Voter,
609 Method to account for arbitrary strains in kinetic Monte Carlo simulations,
610 *Phys. Rev. B* 87 (2013) 144107.
- 611 [41] D. T. Gillespie, A general method for numerically simulating the stochastic
612 time evolution of coupled and chemical reactions, *J. Comput. Phys.* 2 (1976)
613 403.
- 614 [42] A. B. Bortz, M. H. Kalos, J. L. Lebowitz, A new algorithm for Monte Carlo
615 simulation of Ising spin systems, *J. Comput. Phys.* 17 (1975) 10.
- 616 [43] E. Kröner, Die Versetzung als elementare Eigenspannungsquelle, *Z. Natur-*
617 *forsch., A: Phys. Sci.* 11 (1956) 969.
- 618 [44] R. Siems, Mechanical interactions of point defects, *Phys. Stat. Sol.* 30
619 (1968) 645.
- 620 [45] W. G. Wolfer, Segregation of point defects by internal stress fields, in:
621 M. T. Robinson, F. W. Young, Jr. (Eds.), *Fundamental Aspects of Radia-*
622 *tion Damage in Metals*, volume II, p. 812.
- 623 [46] A. I. Ryazanov, D. G. Sherstennikov, Void bias factor in materials with
624 weak cubic anisotropy, *J. Nucl. Mater.* 186 (1991) 33.

- 625 [47] J. L. Tallon, A. Wolfenden, Temperature dependence of the elastic con-
626 stants of aluminum, *J. Phys. Chem. Solids* 40 (1979) 831.
- 627 [48] A. Finel, D. Rodney, Phase field methods and dislocations, in: MRS Fall
628 Meeting Y4.9, Boston, 2000, p. 652.
- 629 [49] S. Y. Hu, L. Q. Chen, Solute segregation and coherent nucleation and
630 growth near a dislocation – a phase-field model integrating defect and phase
631 microstructures, *Acta Mater.* 49 (2001) 463.
- 632 [50] D. Rodney, Y. Le Bouar, A. Finel, Phase field methods and dislocations,
633 *Acta Mater.* 51 (2003) 17.
- 634 [51] J. P. Hirth, J. Lothe, *Theory of Dislocations*, Wiley-Interscience, 1982.
- 635 [52] P. T. Heald, M. V. Speight, Point defect behaviour in irradiated materials,
636 *Acta Metall.* 23 (1975) 1389.
- 637 [53] H. Flyvbjerg, H. G. Petersen, Error estimates on averages of correlated
638 data, *J. Chem. Phys.* 91 (1989) 461.
- 639 [54] G. Kresse, J. Hafner, Ab initio molecular dynamics for liquid metals, *Phys.*
640 *Rev. B* 47 (1993) 558.
- 641 [55] G. Kresse, J. Hafner, Ab initio molecular-dynamics simulation of the liquid-
642 metal amorphous-semiconductor transition in germanium, *Phys. Rev. B* 49
643 (1994) 14251.
- 644 [56] G. Kresse, J. Furthmüller, Efficiency of ab-initio total energy calculations
645 for metals and semiconductors using a plane-wave basis set, *Comp. Mater.*
646 *Sci.* 6 (1996) 15.
- 647 [57] G. Kresse, J. Furthmüller, Efficient iterative schemes for ab initio total-
648 energy calculations using a plane-wave basis set, *Phys. Rev. B* 54 (1996)
649 11169.

- 650 [58] J. P. Perdew, K. Burke, M. Ernzerhof, Generalized gradient approximation
651 made simple, *Phys. Rev. Lett.* 77 (1996) 3865.
- 652 [59] G. Henkelman, B. P. Uberuaga, H. Jansson, A climbing image nudged
653 elastic band method for finding saddle points and minimum energy paths,
654 *J. Chem. Phys.* 113 (2000) 9901.
- 655 [60] V. Spirić, L. E. Rehn, K.-H. Robrock, W. Schilling, Anelastic relaxation
656 due to single self-interstitial atoms in electron-irradiated Al, *Phys. Rev. B*
657 15 (1977) 672.
- 658 [61] W. Schilling, Self-interstitial atoms in metals, *J. Nucl. Mater.* 69 & 70
659 (1978) 465.
- 660 [62] W. G. Wolfer, 1.01 - Fundamental properties of defects in metals, in: R. J.
661 Konings (Ed.), *Comprehensive Nuclear Materials*, Elsevier, Oxford, 2012,
662 p. 1.
- 663 [63] P. T. Heald, The preferential trapping of interstitials at dislocations, *Philos.*
664 *Mag.* 31 (1975) 551.
- 665 [64] C. Jiang, N. Swaminathan, J. Deng, D. Morgan, I. Szlufarska, Effect of
666 grain boundary stresses on sink strength, *Mater. Res. Lett.* 2 (2014) 100.
- 667 [65] W. G. Wolfer, The dislocation bias, *J. Comput. Aided Mater. Des.* 14
668 (2007) 403.
- 669 [66] W. P. Kuykendall, W. Cai, Conditional convergence in two-dimensional
670 dislocation dynamics, *Model. Simul. Mater.* 21 (2013) 055003.
- 671 [67] H. R. Brager, J. L. Straalsund, Defect development in neutron irradiated
672 type 312 stainless steel, *J. Nucl. Mater.* 46 (1973) 134.
- 673 [68] F. A. Nichols, On the estimation of sink-absorption terms in reaction-rate-
674 theory analysis of radiation damage, *J. Nucl. Mater.* 75 (1978) 32.

- 675 [69] J. Hou, X.-S. Kong, X.-Y. Li, X. Wu, C. S. Liu, J.-L. Chen, G.-N. Luo,
676 Modification on theory of sink strength: An Object Kinetic Monte Carlo
677 study, *Comp. Mater. Sci.* 123 (2016) 148.
- 678 [70] H. Rouchette, Sink efficiency calculation of dislocations in irradiated ma-
679 terials by phase-field modelling, Ph.D. thesis, Université de Lille 1, 2015.
- 680 [71] F. S. Ham, Stress-Assisted Precipitation on Dislocations, *J. Appl. Phys.*
681 30 (1959) 915.
- 682 [72] I. G. Margvelashvili, Z. K. Saralidze, Influence of an elastic field of a
683 dislocation on steady-state diffusion fluxes of point defects, *Sov. Phys.*
684 *Solid State* 15 (1974) 1774.
- 685 [73] W. G. Wolfer, M. Ashkin, Diffusion of vacancies and interstitials to edge
686 dislocations, *J. Appl. Phys.* 47 (1976) 791.
- 687 [74] H. Rauh, D. Simon, On the Diffusion Process of Point Defects in the Stress
688 Field of Edge Dislocations, *Phys. Status Solidi A* 46 (1978) 499.
- 689 [75] A. B. Sivak, P. A. Sivak, Efficiency of dislocations as sinks of radiation
690 defects in fcc copper crystal, *Crystallogr. Rep.* 59 (2014) 407.
- 691 [76] H. Rouchette, L. Thuinet, A. Legris, A. Ambard, C. Domain, Influence of
692 shape anisotropy of self-interstitials on dislocation sink efficiencies in Zr:
693 Multiscale modeling, *Phys. Rev. B* 90 (2014) 014104.
- 694 [77] C. H. Woo, Irradiation creep due to elastodiffusion, *J. Nucl. Mater.* 120
695 (1984) 55.
- 696 [78] A. B. Sivak, P. A. Sivak, V. A. Romanov, V. M. Chernov, Effect of external
697 stresses on efficiency of dislocation sinks in BCC (Fe, V) and FCC (Cu)
698 crystals, *Inorg. Mater. Appl. Res.* 6 (2015) 466472.
- 699 [79] A. B. Sivak, P. A. Sivak, V. A. Romanov, V. M. Chernov, Dislocation
700 sinks efficiency for self-point defects in iron and vanadium crystals, *Inorg.*
701 *Mater. Appl. Res.* 6 (2015) 105113.

- ⁷⁰² [80] W. G. Wolfer, M. Ashkin, Stress-induced diffusion of point defects to
⁷⁰³ spherical sinks, J. Appl. Phys. 46 (1975) 547.